An in silico analysis study of the chemical compounds from the crassulaceous plant *Bryophyllumpinnatum (Lam .)*Oken against the SARS-COV-2 proteases

ABSTRACT

Introduction : Acute severe respiratory syndrome SARS-COV-2, a member of the coronavirus family of enveloped RNA viruses, is the disease-causing agent of COVID-19. Research has been done on the active components of medicinal plants that have therapeutic promise. In this regard, the goal of this work was to investigate the anti-SARS-CoV-2 activity of compounds from the plant *Bryophyllumpinnatum* (Lam.) Oken.
Material and Methods : The methodology involved the selection of chemical constituents from the plant leaves in thePubchem database, in addition to obtaining the protein structures of SARS-CoV-2 (6VXX, 6LU7, 1R42) from the Protein Data Bank (PDB). Docking was carried out using Autodock Tools 1.5.6 and AutodockVina, with LigPlus for amino acids and Chimera v.13.1 for3D structures. The most promising compounds were chosen, and the pkCSM tool was used to assess their absorption, distribution, metabolism, excretion and toxicity (ADMET) characteristics.
Results :264 molecular connections were made from the evaluation of 66 chemical components, 21 of which had binding energies that were less than -8.9 kcal.mol-1. The chemical bryotoxin B produced the highest findings with an interaction energy of -9.9 kcal.mol-1 with the Spike protein, indicating its potential as a SARS-CoV-2 inhibitor. These results are encouraging, but more in vitro and in vivo research is needed to validate the effectiveness of COVID-19 treatments.
Conclusion : The molecular docking study shows promising compounds such as Bryotoxin B, β-amyrin acetate and diosmin in B. pinnatum, with high levels of key proteins of SARS-COV-2. ADMET predictions and these compounds were also developed, indicating the therapeutic potential of B. pinnatum as COVID-19 inhibitors.

Keywords:Antiviral activity, Computational chemistry, COVID-19, Medicinal chemistry, Pharmacokinetic properties.

1. INTRODUCTION

The infectious disease caused by the coronavirus, called COVID-19 by the World Health Organization (WHO), was recognized as a global public health emergency in January 2020. The first cases of pneumonia of unknown origin were reported in December 2019 in the city from Wuhan, China [1] . COVID-19 disease is a severe acute respiratory syndrome caused by coronavirus 2 (SARS-CoV-2) [2,3]. Coronaviruses (CoVs) (order *Nidovirales*, family *Coronaviridae*, subfamily *Coronavirinae*) are a family of enveloped RNA viruses. CoVs were the causative agents of two large-scale pandemics in the last two decades, in 2002, Severe

Acute Respiratory Syndrome (SARS) and in 2012, Middle East Respiratory Syndrome (MERS) in Middle Eastern countries . It has a high transmission rate, with contagion occurring mainly through droplets of water and saliva. The infection caused is considered a potentially fatal disease [4] .

Faced with this critical situation of biological safety, which has caused a huge impact on the economy and society, experts have been committed not only to finding new ways to control the spread of the virus between individuals, but also to deepening knowledge about the viral structure of the virus. in order to create more effective therapies. In response to COVID-19, scientists around the world have engaged in intensive research to explore viable therapeutic options that can be rapidly implemented in a cost-effective manner and with a rapid low-cost turnaround [5] .

The need to develop ethnomedicinalphytopharmaceuticals for COVID-19 arises due to the adverse effects of currently repurposed medicines and the long vaccine development process. These phytopharmaceuticals aim to offer treatments that have equal or greater efficacy, along with a more favorable safety profile compared to experimental medicines currently in use for the management of COVID-19 [6].

Currently, computer-based drug design techniques, such as molecular coupling and molecular dynamics, have shown great promise in identifying new compounds with therapeutic potential [7]. Additionally, bioinformatics has allowed the discovery of essential amino acids under almost identical physiological conditions, substantially increasing the reliability of results obtained through computational techniques [8] .

However, depending on the chemical characteristics of the drug and its target receptor, it is possible that new therapeutic options will emerge which, in turn, will save both resources and time [9] . And one of these new resources is the use of medicinal plants, since they are a rich source of chemical compounds with pharmacological properties and can be used as phytotherapeutic resources in different ways, such as infusions, extracts, capsules, ointments, among others, for the relief of symptoms and treatment of various diseases.

In this sense, the species *B. pinnatum (Lam)* Oken belonging to the Crassulaceae family[10] . It is found in tropical Africa, India, China, America and Australia [11,12] . The leaves and leaf juice have been used traditionally as anti-inflammatory, antipyretic, antimicrobial, antioxidant, antitumor, antidiabetic, antiulcer, antiseptic, antihypertensive, hypocholesterolemic, and cough suppressant [13-15] . In clinical studies, *B. pinnatum*leaf extract has demonstrated substantial antimicrobial activity against *Staphylococcus aureus, Escherichia coli* , and *Pseudomonas aeruginosa* at varying levels. These results indicate that *B. pinnatum*leaves have antimicrobial properties that can be exploited for the development of antimicrobial drugs [16] .

In this context, the tools offered by computational methods, such as molecular docking, make it possible to predict the best docking orientation between a compound and its corresponding target protein [17] . This functionality makes it possible to understand the behavior of the compound in the active site of the key protein of a pathogen, as well as to visualize the molecular interactions that occur between the compound and the protein in question [18] . Furthermore, this tool also makes it possible to carry out virtual drug screening and characterize the molecular structures involved, which can be useful in the discovery of new therapeutic compounds. In this way, it is possible to identify compounds with inhibitory potential based on the mechanisms of action in complex with the crystalline structure of the SARS-CoV-2 S protein. Therefore, in order to identify candidate molecules against SARS-Cov-2, we will use a computational study using molecular docking to screen

for compounds from *B. pinnatum*that may function as inhibitors of the S protein of the new coronavirus and evaluate the absorption properties, distribution, metabolization, excretion and toxicity (ADMET) of *B. pinnatum constituents*.

2.MATERIAL AND METHODS

2.1 Kind of study

The present study consists of an in silico analysis of molecular docking and ADMET analysis, the purpose of which was to investigate the interactions of compounds from the B. pinnatum plant with the molecular targets of the SARS-CoV-2 virus, followed by the evaluation of the pharmacokinetic and toxicological characteristics of these compounds.

2.2 Study Location and Duration

All in silico analyzes were conducted in the Medicinal Chemistry and Biotechnology laboratory, located on the campus of the Federal University of Maranhão (UFMA). The research was carried out over a continuous 12-month period. During this interval, the steps of preparing the molecular structures, carrying out the molecular docking simulations, analyzing the ADMET data and interpreting the results were meticulously carried out.

2.3Selection of Ligands

Compounds from various classes originating from the leaves of the species *B. pinnatun (Lam .)* Oken were selected , such as flavonoids, alkaloids, terpenoids , coumarins, saponins, among others, in Scientific databases. Electronic Library Online (Scielo), National Center for Biotechnology information (PubMed), Elsevier group (Scopus) and Google Scholar. The structures were acquired from the Pubchem database (https://pubchem.ncbi.nlm.nih.gov/, accessed on 03 July 2022) for subsequent molecular optimization.

2.4Docagem Molecular

The three-dimensional structures of coronavirus targets were obtained from the PDB protein database (http://www.rcsb.org/, accessed on 10August 2022)[19] , with the respective codes, being: Spike (6VXX), ACE2(1R42) and M^{pro} (6LU7), in addition to designing a Spike interaction complex with ACE2, called receptor 5 [20].For molecular affinity, they were prepared by removing all water molecules and other groups, such as ions, using Chimera v software. 13.1 [21]. Afterwards, polar hydrogen atoms were added, Gasteiger partial charges were calculated and non-polar hydrogens were merged in both parts, using the Autodock Tools (ADT) program version 1.5.6. Performing docking later using the AutoDock program Vina[22]. Using the LIGPLOT program, two-dimensional schematic representations of protein-ligand complexes were generated from the standard PDB file input. Illustrations were obtained of the points of interactions by hydrogen and hydrophobic bonds of the compounds with the amino acids of the viral proteins [23] . The analyzes were concentrated on the lowest energy complexes of the docking conformation. The lowest energy conformation combined with visual inspection was chosen for more detailed analysis [17] .

2.5ADME-TOX Prediction

The analysis of pharmaceutical parameters was performed using the software pkCSM – pharmacokinetics (https://biosig.lab.uq.edu.au/pkcsm/,accessed on 05December 2022), freely available [24] . The *in silico* methodology used with the molecules bryotoxin B, β-amyrin acetate , diosmin , bryophyllin C, friedelin , pseudo taraxasterol ,bryotoxin A, α-amyrin , rutin, bryophyllin A, β- amyrin , psi-taraxasterol , 3,5,7,3′,5′-pentahydroxyflavone, campheritrin , myricitrin , astragalin , quercetin and luteolin . The *in silico* study evaluated the toxicity profile of the most relevant molecules in the post-docking study, including carcinogenicity tests and AMES tests. Among other absorption parameters such as the drug's ability to cross the brain barrier (BBB), as well as the rate of drug absorption (Caco2), the rate of absorption by human intestinal cells (HIA) and excretion (MDCK). Regarding the metabolization process, the inhibition, non-inhibition and substrate formation capacity of the molecules through their behavior in the CYP-450 subfamilies will be evaluated [17,25].

3. RESULTS AND DISCUSSION

3.1 Molecular Docking

*B. pinnatum*were selected through databases to carry out simulations by molecular docking with the ACE2, spike , ACE2/Spike complex (receptor 5) and M^{pro} receptors of SARS-Cov -2, totaling a result of 264 molecular connections (Table 1). The best dockings were considered to be bond energies that obtained values lower than -8.9 $kcal.mol^{-1}$ shown in Table 2 below, resulting in a total of 21 interactions.

Table 1: Results of the 264 dockings carried out involving 66 ligands from the *B. pinnatum species* with the four SARS-CoV-2 proteins.

Parts of the plant	Ligands	ACE2 protein	M^{pro} protein	Spike/ACE2 Complex	Spike Protein	References
		ΔG_{bind} to ($kcal.mol^{-1}$)				
Sheet	Syringic acid ;	-5.0	-5.4	-5.5	-6.0	KAMBOJ;
	Caffeic acid ;	-5.7	-5.7	-6.2	-7.2	SALUJA,
	4-hydroxy-3-methoxy-Cinnamic acid;	-5.4	-5.5	-5.8	-7.1	2009 [26]
	4-hydroxybenzoic acid;	-4.5	-4.8	-5.5	-5.9	
	hydroxycinnamic acid ;	-5.1	-5.2	-5.8	-6.1	
	Ferulic acid ;	-5.4	-5.5	-5.6	-7.0	
	Phosphoenolpyruvate ;	-4.4	-5.1	-5.4	-5.5	
	Astragalin ;	-7.6	-8.4	-7.8	-9.0	
	3,8-dimethoxy-4,5,7-trihydroxyflavone;	-6.8	-7.0	-6.5	-8.1	
	Friedelin ;	-7.9	-8.1	-8.1	-9.3	
	Kaempferol ;	-6.9	-7.8	-6.9	-8.7	
	Taraxerol ;	-7.9	-7.8	-8.0	-8.9	
	Psi-taraxasterol :	-8.2	-7.4	-7.6	-9.1	
	Pseudo taraxasterol ;	-8.4	-7.2	-8.1	-9.3	
	Glutinol ;	-8.3	-8.0	-7.7	-8.8	

	β- sitosterol ;	-6.9	-6.6	-7.1	-7.8	
Folha	Bryophyllin C	-8.4	-8.0	-8.2	-9.3	KHOOSHBU; ANSARI, 2019[27] .
Folha	Bryophyllin B:	-8.5	-6.9	-7.7	-8.4	KAMBOJ;
	Bryophyllin A;	-8.7	-7.9	-8.3	-9.1	SALUJA,
	Bersaldegenin-3-acetate;	-7.6	-7.6	-8.1	-7.9	2009 [26] .
	Bryotoxin A;	-8.7	-8.0	-8.0	-9.2	
	Bryotoxin B;	-8.8	-8.0	-8.1	-9.9	
	Campesterol;	-7.2	-6.4	-7.0	-7.7	
	Isofucosterol;	-7.2	-6.6	-7.1	-7.6	
	Clionasterol	-7.1	-6.4	-7.1	-7.6	
	Codisterol	-7.4	-6.6	-7.2	-8.0	
	Clerosterol	-6.7	-6.4	-7.1	-7.7	
	24-epiclerosterol	-6.6	-6.7	-7.0	-7.8	
	Stigmasterol	-7.4	-6.8	-7.3	-7.9	
	Patuletin	-7.4	-7.3	-7.2	-7.8	
	Palmitic acid	-3.8	-4.2	-5.5	-4.8	
	Oxalic acid	-4.0	-4.1	-4.1	-4.0	
	Citric acid	-5.3	-5.2	-5.9	-6.0	
	Isocitric acid	-5.0	-5.2	-5.5	-6.1	
	Oxaloacetate	-4.2	-4.8	-4.8	-5.0	
	Malic acid	-4.2	-4.8	-4.9	-5.2	
	Succinic acid	-4.0	-4.3	-7.3	-4.7	
	Rutin	-8.2	-8.8	-8.3	-9.1	
	Quercetin	-7.4	-7.5	-7.0	-9.0	
	Luteolin	-7.1	-7.5	-7.2	-9.0	
Folha	Quercitrin	-8.0	-8.9	-7.6	-8.1	TATSIMO et
	Afzelin	-7.6	-8.8	-7.5	-7.6	al., 2012 [28].
	3',4'-dimethoxy Quercetin (Dillenetin)	-6.8	-7.1	-6.9	-8.5	
Aerial	Vanillic acid	-4.9	-5.0	-5.8	-5.9	YADAV;
parts	Phosphoenolpyruvic acid (3,4dihydroxybenzoic acid) or (protocatechuic acid)	-5.1	-5.3	-5.9	-6.4	MISHRA; SINGH, 2021 [29] .
	Stigmast-24-enol	-6.4	-6.5	-7.0	-7.4	
	(24S)-stigmast-25-enol	-6.3	-6.9	-6.2	-7.0	
	(24R)-stigmast-5-enol	-6.4	-6.7	-6.5	-7.1	
Empty	Alpha- Rhamnoisorobin	-8.2	-8.0	-8.2	-8.4	SOBREIRA,

	(Kaempferol-7-rhamnoside)					2013 [30] .
Empty	Kaempferitrin	-8.8	-9.0	-8.3	-8.9	TATSIMO et al., 2012 [28] .
Empty	Myricitrin	-7.9	-9.0	-7.8	-8.3	FÜRER et
Flower	Isoquercitrin	-7.6	-8.1	-8.1	-8.0	al., 2016 [31]
	Miquelianin (Quercetin-3-O-glucuronide)	-7.8	-8.0	-8.5	-8.4	.
Whole plant	3,5,7,3',5'-Pentahydroxyflavone	-7.0	-7.3	-6.9	-9.1	
Sheet	Apigenin	-6.7	-7.7	-7.0	-8.6	YADAV; MISHRA; SINGH, 2021 [29] .
Sheet	Diosmin	-9.4	-9.0	-8.3	-9.4	FÜRER et al., 2016 [31] .
Sheet	Gamma butyrolactone	-3.6	-3.8	-3.8	-3.9	UCHEGBU et
	3,4 – Epoxytetrahydrothiophene-1,1dioxide	-3.8	-4.2	-4.1	-4.7	al., 2017 [32] .
	1-Octen-3-ol	-3.4	-3.9	-4.5	-4.7	
	3,5-Dihydroxy-6-methyl-2,3-dihydro-4H-pyran-4-one	-4.6	-5.1	-4.9	-5.5	
	Benzaldehyde	-4.2	-4.2	-5.0	-4.9	
	Alpha-D- Glucopyranoside, methyl	-4.8	-5.2	-5.3	-6.0	
	Oleic acid	-4.9	-4.3	-6.0	-5.5	
Sheet	α- amyrin	-9.2	-7.9	-8.0	-9.0	KAMBOJ;
	β- amyrin	-8.1	-7.2	-8.1	-9.1	SALUJA,
	β- amyrin acetate	-8.4	-7.6	-7.9	-9.5	2009 [26] .

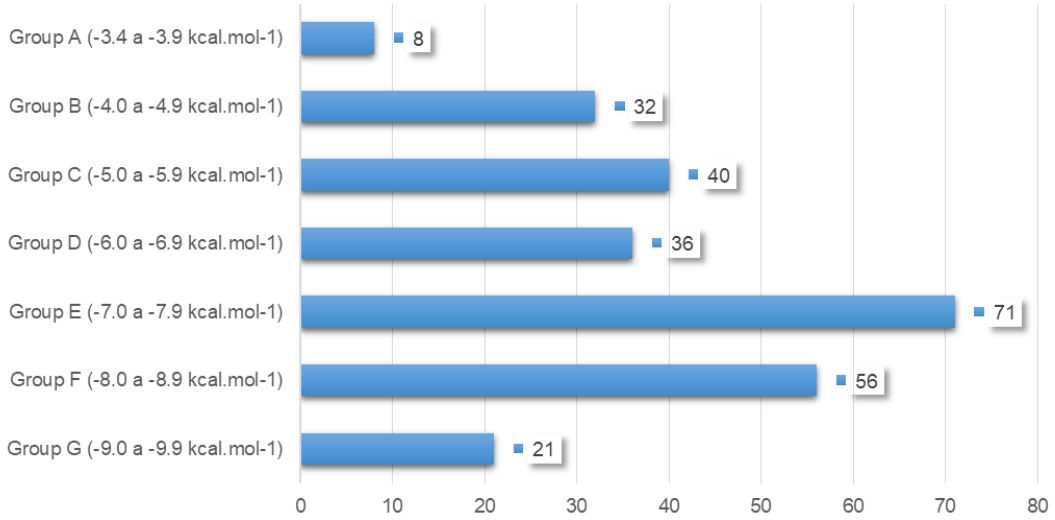

Source: Own authorship, 2023.

Figure 1: Results of the 264 molecular dockings.
Source: Own authorship, 2023.

Figure 1 shows the 264 dockings carried out in this work, with binding energies varying from -9.9 kcal.mol-1 to -3.4 kcal.mol^{-1}. Group E showed a greater number of interactions compared to the other groups (71 interactions), in the range of -7.0 kcal.mol^{-1} to -7.9 kcal.mol^{-1}. Group A presented a lower number of interactions (eight interactions), in the range of -3.4 kcal.mol^{-1}to -3.9 kcal.mol^{-1}. Groups B, C and D presented a number of close interactions in the range of 30 to 40 interactions (group B: 32 interactions; group C: 40 interactions; group D: 36 interactions). Group F showed satisfactory results, both in quantity and interaction energies, presenting 56 interactions in the range of -8.0 kcal.mol^{-1} to -8.9 kcal.mol^{-1}. Group G is the most satisfactory in this study, as it presented the lowest number of molecular interactions, ranging from -9.0 kcal.mol^{-1} to -9.9 kcal.mol^{-1}, presenting 21 molecular interactions between the constituents and proteins. The results in Table 2 show that the best molecular interactions with proteins were observed in 18 different ligands (Figure 2).

Table 2: Molecular affinity parameters of the chemical constituents (ligands) of the species *B. pinnatum*, with the proteins ACE2, Spike, Spike/ACE2 complex and M^{pro} of the new coronavirus (COVID-19) with binding energy results lower than -8.9 kcal.mol^{-1}.

No.	Complex (Protein-Bind)	ΔG $_{bind}$ ^{to} (kcal.mol $^{-1}$)	Amino acids that interacted by hydrogen bonding	Amino acids that interacted by hydrophobic bond
1	Bryotoxin B/Spike	-9.9	Asp428	Phe464, Thr430, Ser514, Asp198, Phe515, Glu516, Leu518, Leu517, Arg983, His519, Ser974, Ile973
2	β- amyrinacetate/Spike	-9.5	His519	Asp979, Ile973, Leu518, Glu516,

				Tyr200, Asp198, Thr430, Leu517, Arg983, Phe515, Val976, Ser974, Arg567
3	Diosmin/Spike	-9.4	Ser967, Ser968, Leu754, Ile569, Asp568, Ile973, Arg983	His49, Gly757, Gln755, Asn969, Leu517, Ser974, Asp571, Arg567
4	Diosmin/ACE2	-9.4	Glu375, Glu402, Tyr385, Arg393, Asp350, Ser44, Ala348	Asn394, Asp382, Phe40, Ser47, Trp349, Asn51, Val343, Thr347, His378, His401
5	Bryophyllin C/Spike	-9.3	Asp428	Ser514, Asp198, Phe464, Thr430, Glu516, Phe515, Leu517, Leu518, His519, Arg983, Ser974, Ile973
6	Friedelin/Spike	-9.3		Ser974, Ile973, Asp428, Asp198, Thr430, Phe429, Pro426, Glu516, Leu517, Phe515, Leu518, His519, Arg983
7	Pseudo taraxasterol/Spike	-9.3	Asp198	Arg983, Leu517, Leu518, Glu516, Phe515, Thr430, Phe464, Pro426, Ser514
8	Bryotoxin A/Spike	-9.2	Arg983, Thr430	Ser975, Asp571, His519, Ile973, Ser974, Leu517, Leu518, Asp198, Asp428, Phe429, Pro426, Tyr200, Glu516, Ser514, Phe515
9	α- amyrin/ACE2	-9.2	Tyr385	Ser47, Ala348, Phe40, Asp382, Asn394, His401, Asp350, Trp349, Asn51, Thr347
10	Rutin/Spike	-9.1	Ile569, Asp568, Ser967, Ser968, Leu754, Ser975, Asn969, Thr51, Ser50, Gln52, His49	Asp571, His519, Arg567, Gln755, Gly757

11	Bryophyllin A/Spike	-9.1	Asp428	Arg983, Thr430, Asp198, Ser514, Phe515, Phe464, Glu516, Leu518, Leu517, His519
12	β-amyrin/Spike	-9.1		Phe464, Tyr200, Thr430, Asp428, Arg983, Ile973, Leu518, Glu516, Asp198
13	Psi-taraxasterol/Spike	-9.1		Leu518, Arg983, Leu517, Phe464, Thr430, Phe515, Phe429, Ser514, Pro426, Asp198, Asp428, Glu516
14	3,5,7,3′,5′-Pentahydroxyflavone/Spike	-9.1	Thr573, Phe855, Met740, Gly744, Tyr741, Arg1000, Leu977, Thr549	Phe541, Ile587, Pro589, Gly548, Thr572, Asn856
15	Kaempferitrin/ M^{pro}	-9.0	Thr190, Gln192, Arg188, Glu166, Gly143, Thr26	Pro168, Met165, His41, Gln189, Met49, Leu27, Thr25, Cys145, Asn142
16	Myricitrin/M^{pro}	-9.0	Glu166, Asp187, Tyr54, His163, Asn142, Leu141, Ser144	His164, Met165, Arg188, Met49, His41, Gln189, Gly143, Cys145
17	Astragalin/Spike	-9.0	Ile587, Asp568, Asn856, Met740, Ile742, Arg1000, Thr547, Thr573	Phe855, Gly744, Tyr741, Asn978, Gly548, Leu546, Pro589, Thr572
18	Quercetin/Spike	-9.0	Arg1000, Leu977, Thr573, Tyr741, Phe855	Asn856, Gly744, Leu966, Val976, Thr547, Met740, Thr572, Asn978, Leu546

19	Luteolin/Spike	-9.0	Tyr741, Met740, Phe855, Thr573, Arg1000	Gly744, Asn856, Gly548, Thr547, Leu546, Thr572, Val976, Asn978, Leu966
20	α-amyrin/Spike	-9.0		Asp198, Phe515, Asp428, Arg983, Thr430, Leu517, Ile973, Leu518, Tyr200,
21	Diosmin/ M^{pro}	-9.0	Tyr54, Thr190, His164, Thr26	Asp187, Met49, His41, Leu27, His163, Thr25, Arg188, Met165, Gln189, Glu166, Leu141, Asn142, Cys145, Gly143, Thr24

Source: Own authorship, 2023.

1)


OH

2)

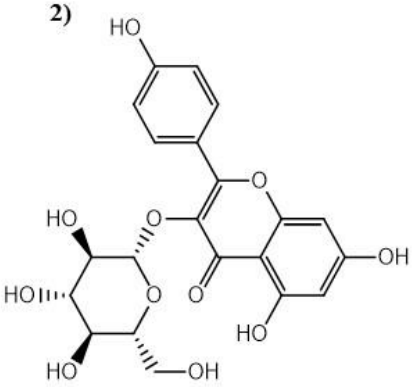
HO
O
HO
O
HO
O
OH
O
HO
HO
OH

3)

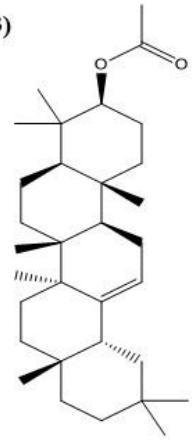
O
O

4)

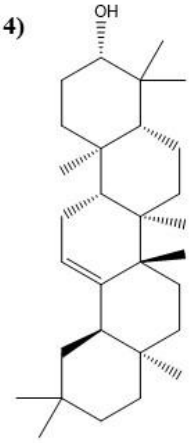
OH

5)

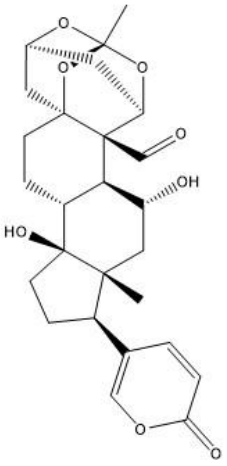
O
O
O
O
OH
HO
O
O

6)

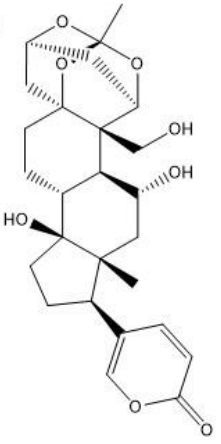
O
O
O
OH
OH
HO
O
O

7)

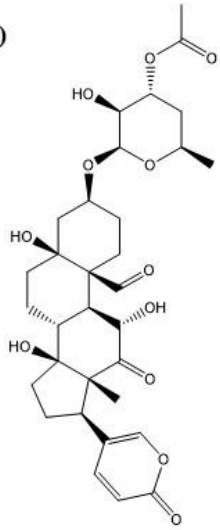
O
O
HO
O
HO
O
OH
HO
O
O
O

8)

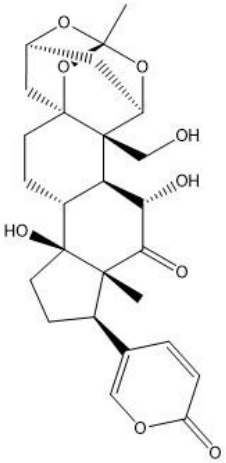
O
O
O
OH
OH
HO
O
O
O

9)

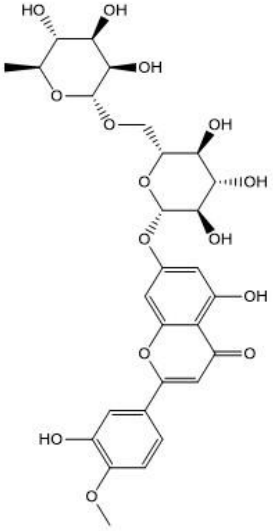
HO
OH
OH
O
O
OH
O
OH
OH
O
OH
O
HO
O

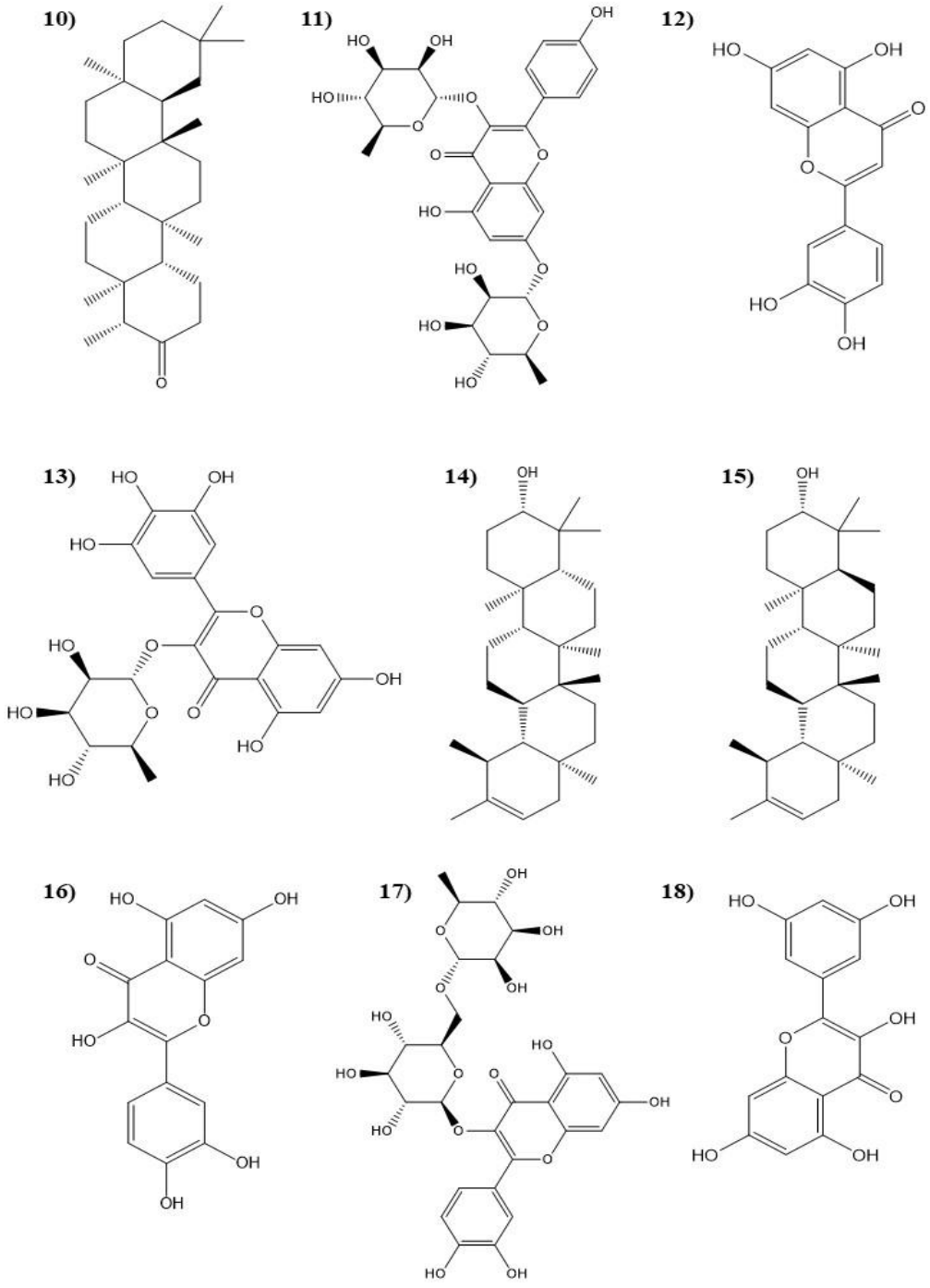

Figure2: Two-dimensional (2D) structures of the molecules that showed the best results in molecular interaction. [1 (α-Amyrin); **2**(Astragalin); **3** (β-Amyrin acetate); **4** (β-Amyrin); **5** (Bryophyllin A); **6** (Bryophyllin C); **7** (Bryotoxin A); **8** (Bryotoxin B); **9** (Diosmin);

10(Friedelin); **11** (Kaempferitrin); **12** (Luteolin); **13** (Myricitrin); **14** (Pseudo taraxasterol); **15** (Psi-taraxasterol); **16** (Quercetin); **17** (Rutin); **18** (3,5,7,3′,5′-Pentahydroxyflavone)**]**

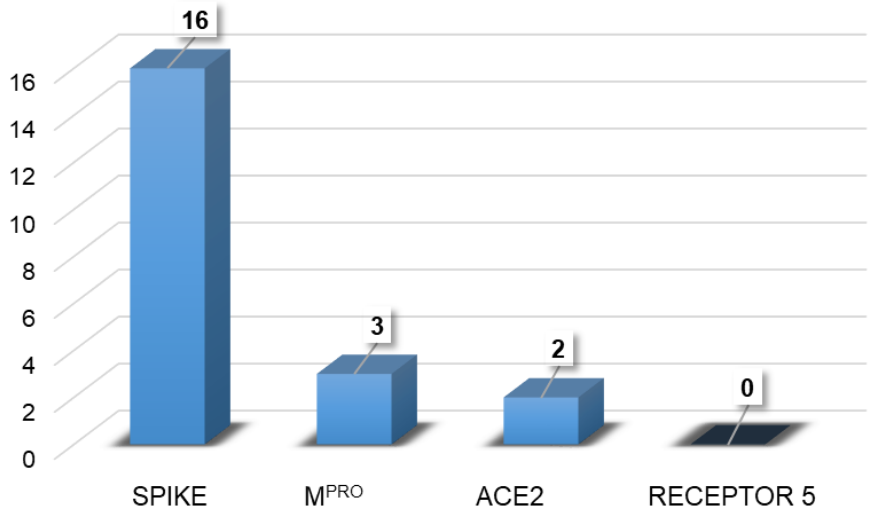

Source: Own authorship, 2023.

Figure 3: Better molecular interactions

Source: Own authorship, 2023.

Within the parameter established for the initial analysis of the 21 couplings (Figure 3), sixteen dockings had the involvement of the Spike protein, while three dockings were the result of the ligand coupling with the M^{pro} protein and two results with satisfactory binding energy were with the ACE2 protein. However, the lowest binding energy obtained in the docking performed on receptor 5 did not reach the energy parameter that was initially established to analyze the best interaction energies, with the best result obtained being the involvement of the myquelianine ligand with the ACE2 complex/Spike (receptor 5), resulting in a binding energy of -8.5 $kcal.mol^{-1}$(Table 1), which is also considered to have excellent interactional energy.

The Spike protein presented excellent molecular affinity results, the sixteen interactions with their respective binding energies involved the following compounds: bryotoxin B (-9.9 $kcal.mol^{-1}$), β- amyrin acetate (-9.5 $kcal.mol^{-1}$), diosmin (-9.4 $kcal.mol^{-1}$), bryophyllin C (-9.3 $kcal.mol^{-1}$), friedelin (-9.3 $kcal.mol^{-1}$), pseudo taraxasterol (-9.3 $kcal.mol^{-1}$), bryotoxin A (-9.2 $kcal.mol^{-1}$), rutin (-9.1 $kcal.mol^{-1}$), bryophyllin A (-9.1 $kcal.mol^{-1}$), β-amyrin (-9.1 $kcal.mol^{-1}$), psi-taraxasterol (-9.1 $kcal.mol^{-1}$), 3,5,7,3′,5′-pentahydroxy-flavone (-9.1 $kcal.mol^{-1}$), astragalin

(- 9.0 kcal.mol^{-1}), quercetin (-9.0 kcal.mol^{-1}), luteolin (-9.0 kcal.mol^{-1}) and α- amyrin (-9.0 kcal.mol^{-1}).

Coronavirus M^{pro}protein , the results were the same, for the molecular interactions in the compounds : campferitrin , myricitrin and diosmin . In both molecular interactions with these compounds, a ligand binding energy with the protein of -9.0 kcal.mol^{-1} was obtained, also resulting in an excellent interaction energy.

In the ACE2 protein, which is widely expressed in human organs, such as the heart and kidneys, as well as in the main target cells of SARS-CoV-2, the alveolar epithelial cells of the lung [33], it showed couplings with the compounds diosmin and α- amyrin , resulting in excellent binding free energies. For the diosmin ligand , an interaction energy of -9.4 kcal.mol^{-1} was obtained, and for the α- amyrin ligand , it resulted in an interaction energy equal to -9.2 kcal.mol^{-1}.

The most satisfactory interactions, according to the parameter that was analyzed in the molecular dockings, were with the involvement of the Spike protein and ACE2. The Spike protein stands out, presenting the three best levels of molecular affinity with the following compounds analyzed in computer simulation (Table 2): bryotoxin B, β- amyrin acetate and diosmin .

The interaction of the bryotoxin B compound with the Spike protein resulted in the best binding energy among the dockings carried out, of -9.9 kcal.mol^{-1}(Figure 4), which interacted by hydrogen bonding with an amino acid (Asp428), and interacted with twelve amino acids per hydrophobic bond (Phe464, Thr430, Ser514, Asp198, Phe515, Glu516, Leu518,Leu517, Arg983, His519, Ser974, Ile973). Bryotoxin B is a chemical compound found in *B. pinnatum*that also has herbal potential in suppressing the activity of adenosine monophosphate and inducible nitric oxide synthase, which play a role in thickening and inflammation in atherosclerosis disease [34].According to Rahman et al., (2022) [35], active compounds from B. pinnatum, such as Bryotoxin A and Bryophyllum B, demonstrate promising potential as COVID-19 inhibitors, being able to modulate the immune response and prevent cytokine storms.

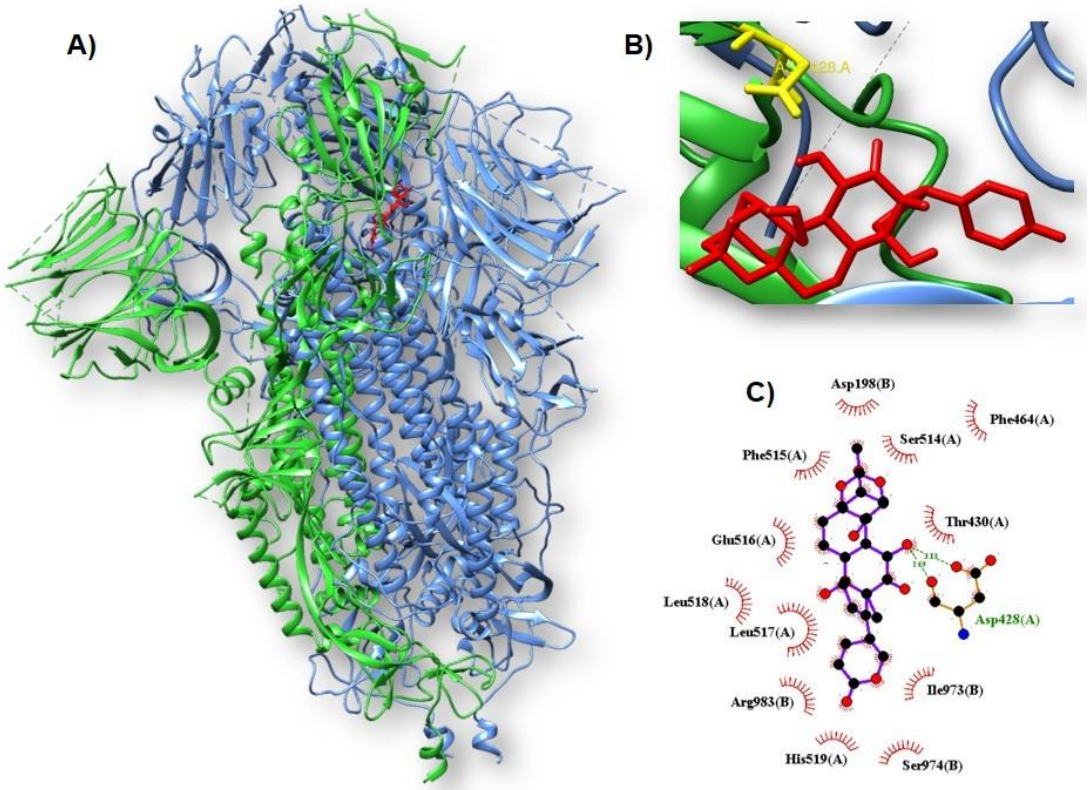

Figure 4: Molecular coupling of the bryotoxin B ligand (red) with the Spike protein obtaining binding free energy of -9.9 kcal.mol^{-1}. A) Site of interaction of the protein-ligand complex. B) 3D conformation of the active site of the binding of the bryotoxin B compound with the Spike (S) protein. C) 2D scheme showing hydrogen bonds and hydrophobic interactions.

Source: Own authorship, 2023.

The involvement of β- amyrin acetate with the Spike protein, being the second best result, presented a binding energy of -9.5 kcal.mol^{-1}, which interacted by hydrogen bonding with an amino acid (His519), and interacted with thirteen amino acids by hydrophobic bond (Asp979, Ile973, Leu518, Glu516, Tyr200, Asp198, Thr430, Leu517, Arg983, Phe515, Val976, Ser974, Arg567). β-Amyrin acetate has pharmacological properties as a potent inhibitor of α-glucosidase[36], as well as demonstrating properties as a potent lipid-lowering agent[37] .

The interaction of the diosmin compound with the Spike protein, third best result, obtained an interaction energy of the ligand with the protein of -9.4 kcal.mol^{-1}, which interacted via hydrogen bonding with seven amino acids (Ser967, Ser968, Leu754, Ile569, Asp568, Ile973, Arg983), and interacted with eight amino acids by hydrophobic bond (His49, Gly757,

Gln755, Asn969, Leu517, Ser974, Asp571, Arg567). Diosmin is a plant-derived flavone glycoside that has antioxidant, anticancer, antidiabetic, antibacterial properties, and has therapeutic action for a variety of disorders, reducing oxidative stress, altering the activity of specific enzymes and promoting apoptosis in a variety of cancer cell lines [38].

With the ACE2 protein, the diosmin compound presented a favorable binding energy, resulting in an energetic value of -9.4 kcal.mol^{-1}(Figure 5), obtaining the same interaction value with the Spike protein. It interacted by hydrogen bonding with seven amino acids (Glu375, Glu402, Tyr385, Arg393, Asp350, Ser44, Ala348), and interacted with ten amino acids by hydrophobic bond (Asn394, Asp382, Phe40, Ser47, Trp349, Asn51, Val343, Thr347, His378 , His401).

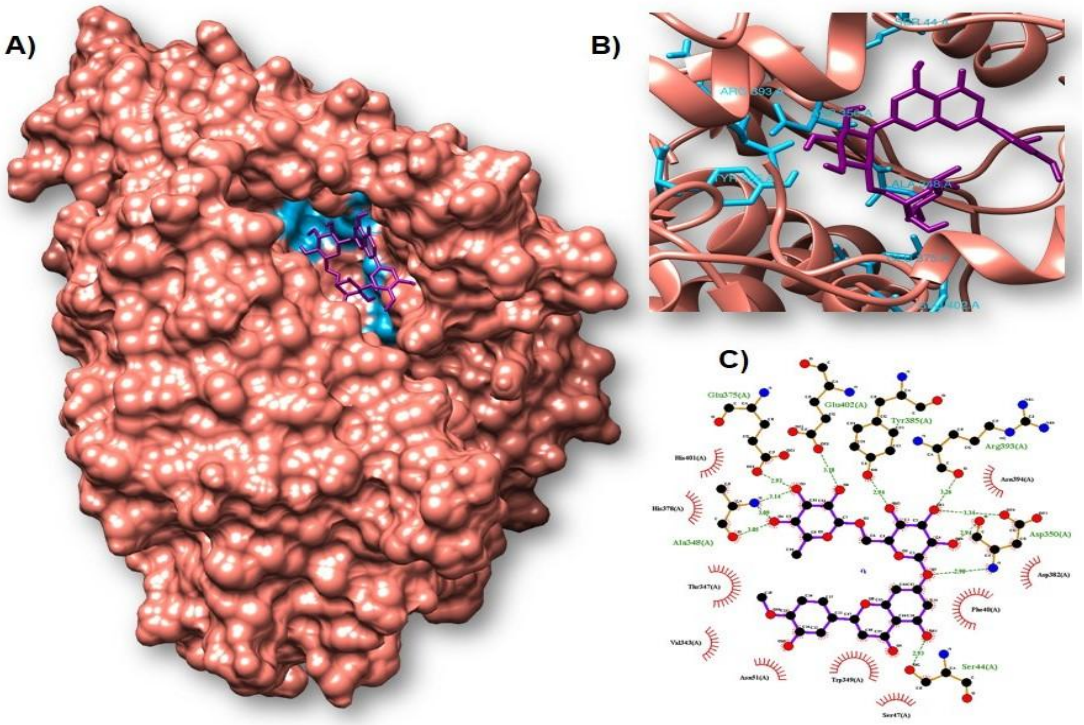

Figure 5: Molecular coupling of the diosmin ligand (violet) with the ACE2 protein obtaining binding free energy of -9.0 kcal.mol^{-1}. A) Site of interaction of the protein-ligand complex. B) 3D conformation of the active site of the diosmin compound binding to the ACE2 protein. C) 2D scheme showing hydrogen bonds and hydrophobic interactions.

Source: Own authorship, 2023.

Diosmin has antioxidant and anti-inflammatory properties, as well as hepatoprotective properties .[39] , protects against changes in antioxidant expression, body and organ weight and histopathology caused by cadmium, increases the expression of antioxidant enzymes and reduces the production of inflammatory cytokines, protects against alcohol-induced abnormalities, decreases liver abnormalities [38] , has anti-hyperglycemic activity , stimulating the production of insulin from existing β-cells of the pancreas [40] and also has antiproliferative effects in human colon cancer cell lines [41] .

In this molecular docking study to prospect the antiviral activity of the chemical constituents of *B. pinnatum (Lam .)* Oken , the two main glycoproteins of the SARS-CoV-2 capsid were used, which perform the binding and entry process into the host cell and carry out the interaction that facilitates viral infection, being the Spike glycoprotein and the main proteinase (M^{pro}) .

The molecule that obtained the best interaction in the molecular docking process with the main protein (M^{pro}) was the diosmin ligand , with a value of -9.4 $kcal.mol^{-1}$(Figure 6). It interacted by hydrogen bonding with four amino acids (Tyr54, Thr190, His164, Thr26), and interacted with fifteen amino acids by hydrophobic bond (Asp187, Met49, His41, Leu27, His163, Thr25, Arg188, Met165, Gln189, Glu166, Leu141, Asn142 , Cys145, Gly143, Thr24).

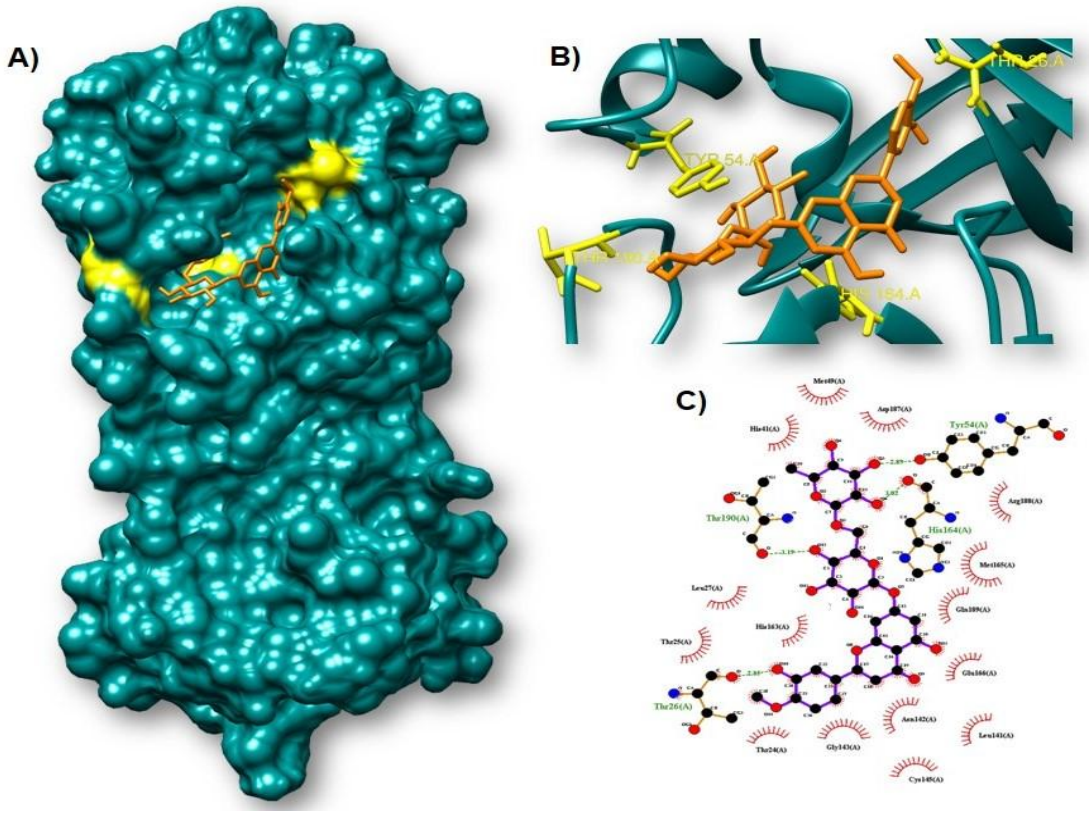

Figure 6: Molecular coupling of the diosmin ligand (orange) with the M^{pro} protein obtaining binding free energy of -9.4 $kcal.mol^{-1}$. A) Site of interaction of the protein-ligand complex. B) 3D conformation of the active site of the diosmin compound

binding to the M^{pro} protein . C) 2D scheme showing hydrogen bonds and hydrophobic interactions.
Source: Own authorship, 2023.

A recognized receptor for coronavirus treatment is M^{pro} or Main protease, also known as 3CLpro [42,43] . This protein processes the 1ab polyprotein into mature nonstructural proteins that are essential for virus replication in the host [44] . Also, human proteases with the same specificity have not been discovered so far, making M^{pro} an ideal receptor for treating coronavirus infections [45] .

In the molecular docking process carried out with target receptor 5 (Spike/ACE2 complex), the best interaction was obtained with the ligand Miquelianine , with a binding energy of -8.5 $kcal.mol^{-1}$ as shown in Figure 7.

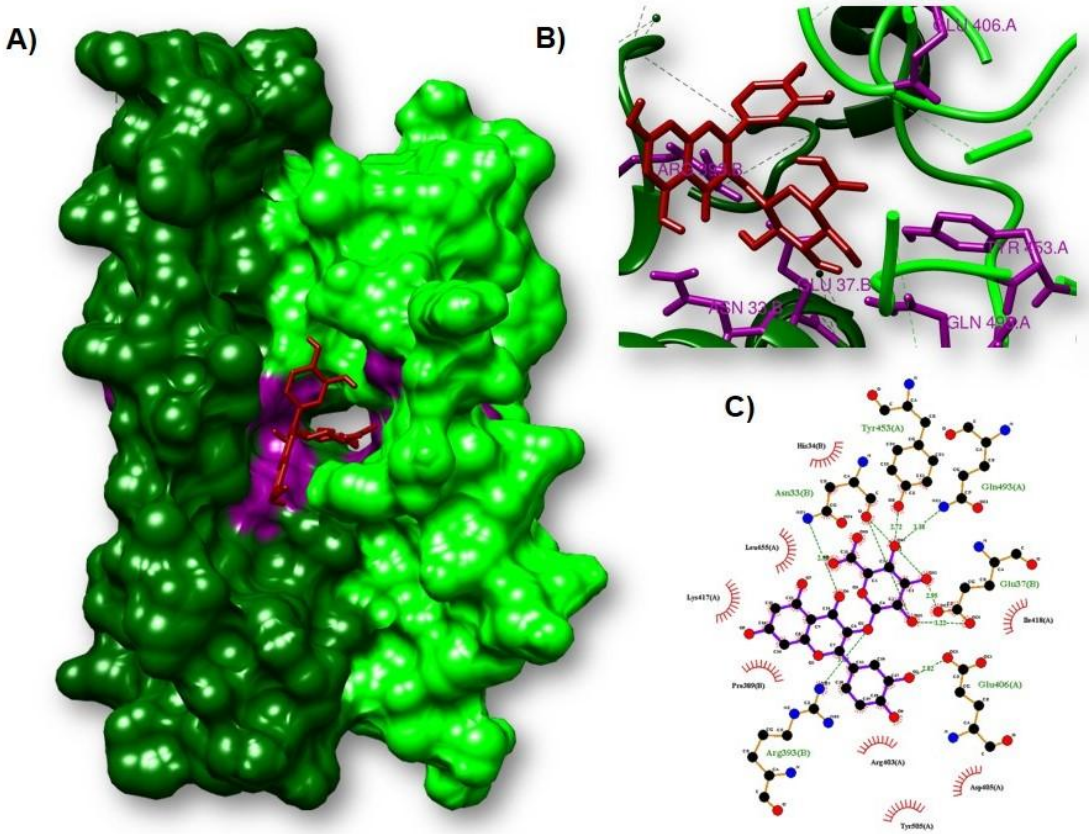

Figure 7: Molecular coupling of the Myquelianine ligand (red) with the Spike/ ACE2 complex obtaining binding free energy of -8.5 $kcal.mol^{-1}$. A) Site of interaction of the protein-ligand complex. B) 3D conformation of the active site of the binding of the myquelianine compound with the Spike/ACE2 complex. C) 2D scheme showing hydrogen bonds and hydrophobic interactions.
Source: Own authorship, 2023.

Created in 1999, the National Health Surveillance Agency (ANVISA) regulates medicines for human use, pharmaceutical inputs, medical and hospital devices, foods, cosmetics and

sanitizers [46, 47] . Anvisa evaluates the more technical aspects of clinical research, that is, it evaluates in more depth the quality of the experimental medicine, regarding its production, quality control and evaluation of stability studies, among other aspects [48] .

With the aim of finding an emergency and appropriate treatment for COVID-19, numerous studies were conducted to identify drugs that would perform a satisfactory and efficient antiviral action. During the period between 2021 and 2022, the National Health Surveillance Agency (ANVISA) approved four drugs for this purpose: remdesivir, paxlovid , molnupiravir and baricitinib[49] . These drugs were subjected to molecular docking studies to evaluate their ability to inhibit SARS-CoV-2 proteases, the results of which are shown in Table 3.

Table 3: Molecular affinity parameters of the drugs Baricitinib, Molnupiravir , Paxlovid and Remdesivir with the ACE2, M^{pro} , ACE2/S Complex and Spike proteins of the new coronavirus (COVID-19).

DRUG	CID	ACE2	M^{PRO}	Spike/ACE2 Complex	Spike
Remdesivir	121304016	-7.3	-7.9	-7.6	-7.5
Paxlovid (Nirmatrelvir + Ritonavir)	155903259	-7.1	-7.6	-7.0	-7.3
Molnupiravir	145996610	-7.2	-6.7	-6.8	-7.9
Baricitinib	44205240	-6.8	-7.9	-7.8	-8.0

Source: Own authorship, 2023.

During the molecular docking analysis, both remdesivir and paxlovid demonstrated the best interaction energy with the M^{pro} protein , presenting values of -7.9 kcal.mol^{-1} and -7.6 kcal.mol^{-1}, respectively (Table 3). However, when compared, compounds such as Kaempferitrin , myricitrin and diosmin exhibited a higher interaction energy than remdesivir and paxlovid with the M^{pro} protein , obtaining a value of -9.0 kcal.mol^{-1}. Regarding the molecular docking of the other two drugs, both molnupiravir and baricitinib demonstrated a high affinity for interaction with the Spike protein, presenting energy values of -7.9 kcal.mol^{-1} and -8.0 kcal.mol^{-1}, respectively (Table 3). However, when compared with the compound bryotoxin B, which, when interacting with the Spike protein, obtained a binding energy of -9.9 kcal.mol^{-1}, both drugs showed a lower interaction energy.

3.2 ADME-TOX PREDICTION

The analysis of bioactivity and pharmacokinetic indices in relation to ADMET properties (absorption, distribution, metabolism, excretion and toxicity) is intrinsically linked to the fate of chemical substances in the human body, reflecting their interactions with organs. Prediction of ADMET properties is crucial, especially for exogenous substances consumed in prolonged or high concentrations [50] .

In silico ADMETstudies have become more relevant by reducing the risks of development failures, focusing attention on promising compounds. This computational approach also makes optimizations in drug discovery costs and time, resulting in notable benefits [51] . The absorption prediction parameters of the molecules that demonstrated significant binding energies with the SARS-COV-2 proteins are described in Table 4.

Table 4: Absorption properties of *B. pinnatum compounds* with the best molecular interaction energies.

Compounds	Absorption					
	Solubility in water (log mol/l)	**P $_{Caco2}$ (Log Papp at $^{10-6}$ cm/s)**	**AIH %**	**Skin permeability (log of Kp)**	**P-glycoprotein I inhibitor**	**P-glycoprotein II inhibitor**
Astragalin	-3,365	-0.497	42,196	-2,735	No	No
Bryophyllin A	-3,982	0.665	95,834	-3,351	No	No
Bryophyllin C	-3,912	0.6	90,619	-3,219	No	No
Bryotoxin A	-4,393	0.571	54,147	-2,781	Yes	No
Bryotoxin B	-4,139	1,065	83,761	-2,948	No	No
Diosmin	-3,036	-0.291	33,146	-2,735	No	No
Friedelin	-5,856	1,236	97,452	-2,722	Yes	Yes
Kaempferitrin	-3,059	-0.336	30,054	-2,735	No	No
Luteolin	-3,173	0.762	81,082	-2,735	No	No
Myricitrin	-2,943	-0.694	51,296	-2,735	No	No
Pseudo taraxasterol	-6,439	1,226	95,227	-2,814	Yes	Yes
Psi-taraxasterol	-6,439	1,226	95,227	-2,814	Yes	Yes
Quercetin	-2,982	0.694	74.84	-2,735	No	No
Rutin	-2,909	-0.662	25,454	-2,735	No	No
α-amyrin	-6,436	1,221	94,053	-2,815	Yes	Yes
β-amyrin	-6,467	1,221	93,724	-2,813	Yes	Yes
β-amyrin acetate	-6,623	1,209	95,939	-2,811	Yes	Yes
3,5,7,3′,5′-Pentahydroxyflavone	-3,064	0.671	69,906	-2,735	No	No

Source: Source: Own authorship, 2023.

Note: PCaco-2: Caco-2 cell permeability; AIH: human intestinal absorption potential; PSkin : skin permeability; IGp -P: P-glycoprotein inhibitor; VDss : volume of distribution at steady state; PBH: blood-brain barrier permeability.

The analyzed compounds revealed a water solubility ranging from -5 to -1 (mol/L), which is favorable for their hydrophilic capacity and subsequent passage through the plasma membrane [52] . However, exceptions were observed for β- amyrin acetate , the pseudo

taraxasterol , α- amyrin and Psi-taraxasterol , which presented solubility values below -6 (mol/l).

The Caco-2 permeability technique employs cells derived from human colon adenocarcinoma, which exhibit similarities with the human intestinal epithelium. This makes it possible to predict the absorption of orally administered drugs in humans *in vivo*[53] . In this context, a compound is classified as having high permeability by Caco-2 if its predictive value is greater than 0.90 cm/s [24,54] .

In the analysis, the compounds that demonstrated high permeability to Caco-2 were: bryotoxin B (1,065 cm/s), β- amyrin acetate (1,209 cm/s), friedelin (1,236 cm/s), pseudo taraxasterol (1,226 cm/s), α- amyrin (1,221 cm/s), β- amyrin (1,221 cm/s) and psi-taraxasterol (1,226 cm/s).

The absorption of compounds from the gastrointestinal tract is affected by the water/liposolubility ratio, unlike drugs that do not need to go through the pre -systemic biotransformation process. Human intestinal absorption – AIH (%) is classified as follows: poorly absorbed compounds have an AIH of 0 to 20%; moderately absorbed compounds exhibit an AIH of 20 to 70%; and well-absorbed compounds have an AIH of 70 to 100% [55] . During the analysis, it was found that 11 of the 18 compounds presented values ranging from 74.84% to 97.45%, which indicates a good potential for intestinal absorption. On the other hand, the other 7 compounds presented values ranging from 25.45% to 69.90%, showing a potential for moderate intestinal absorption.

Skin permeability is essential in the development of transdermal drug delivery systems. Compounds with log Kp> -2.5 cm/h are considered to have moderately low skin permeability [54] . Most permeability values through human skin were in the range of -3,351 cm/h to -2,735 cm/h; therefore, the compounds cannot be absorbed through human skin [17] .

P-glycoprotein limits the oral absorption of some drugs, as it effects the efflux of drug molecules out of cells, reducing the effective concentration of these drug molecules [56] . Among the compounds analyzed, only six demonstrated inhibition of both P-glycoprotein I and P-glycoprotein II (β- amyrin acetate , friedelin , pseudo taraxasterol , α- amyrin , β-amyrin and psi-taraxasterol) while only one compound exclusively inhibited glycoprotein -PI (bryotoxin A).

The VDss (volume of distribution at steady state) represents the volume of body fluid necessary to dissolve the same concentration of drug present in blood plasma [51] . The volume of distribution (VDss) directly influences the amount of drug that reaches the tissues. Log VDss values less than -0.15 indicate a low volume of distribution, with greater concentration in blood plasma, while values greater than 0.45 suggest a high volume of distribution, with wide distribution in tissues beyond blood plasma [54] (Table 5).

Table 5: Distribution properties of *B. pinnatum compounds* with the best molecular interaction energies.

Compounds	Distribution	
	VDss (human) (log L/Kg)	PBH (BB log)
Astragalin	-0.498	-1,993
Bryophyllin A	0.199	-0.816
Bryophyllin C	0.177	-1,155
Bryotoxin A	0.147	-1,4
Bryotoxin B	0.339	-1,164

Diosmin	0.005	-2,286
Friedelin	-0.023	0.73
Kaempferitrin	-0.569	-2.104
Luteolin	0.071	-1,199
Myricitrin	-0.271	-2,324
Pseudo taraxasterol	0.265	0.687
Psi-taraxasterol	0.265	0.687
Quercetin	0.31	-1,377
Rutin	-0.155	-2,556
α- amyrin	0.258	0.678
β- amyrin	0.26	0.67
β- amyrin acetate	0.131	0,607
3,5,7,3′,5′-Pentahydroxyflavone	0.168	-1.354

Source: Own authorship, 2023.

Note: VDss : volume of distribution at steady state; PBH: blood-brain barrier permeability.

According to the analysis results, the compounds listed with the best positive log VDss values , such as bryotoxin B, β- amyrin acetate , pseudo taraxasterol , bryotoxin A, α- amyrin , β- amyrin , psi-taraxasterol , 3,5,7,3′,5′-Pentahydroxyflavone and quercetin, have moderate potential to reach different tissues in the body. On the other hand, compounds with log VDss very close to or below 0, such as diosmin , friedelin , rutin, kaempferitrin , myricitrin and astragalin , indicate a lower tissue distribution.

The potential for crossing the blood-brain barrier (BBB) is indicated by log BB. Values above 0.3 suggest that the substance can cross the BBB effectively, while molecules with log BB above – 1 have difficulty distributing properly in the brain [57] . Compounds with the best log BB values, such as β- amyrin acetate , friedelin , pseudo taraxasterol , α- amyrin and psi-taraxasterol demonstrate a positive potential to cross the blood-brain barrier, indicating their ability to be distributed more effectively in brain tissue .

CYP450 constitutes a superfamily of enzymes that play a crucial role in drug metabolism. The CYO450 enzyme is responsible for metabolizing more than 80% of drugs during the first pass process through the liver, contributing to their detoxification, therefore, any compound that inhibits CYP450 enzymes can result in toxicity [58] . Given that drugs often require oxidation to produce the desired therapeutic effect and be excreted from the body, the interaction with CYP450 enzymes must be carefully considered. Within this superfamily, there are five distinct isoforms (CYP 3A4, 2D6, 1A2, 2C9 and 2C19) of CYP450 [59] (Table 6).

Table 6: Metabolism and excretion properties of *B. pinnatum compounds* with the best molecular interaction energies.

Compounds	**Metabolism**							**Excretion**
	CYP2D6 substrate	**CYP3A4 substrate**	**CYP1A2 inhibitor**	**CYP2C19 inhibitor**	**CYP2C9 inhibitor**	**CYP2D6 inhibitor**	**CYP3A4 inhibitor**	**OCT2 Renal Substrate**
Astragalin	No	No	No	No	No	No	No	No

Bryophyllin A	No	Yes	No	No	No	No	No	No
Bryophyllin C	No	No	No	No	No	No	No	No
Bryotoxin A	No	Yes	No	No	No	No	No	No
Bryotoxin B	No	No	No	No	No	No	No	No
Diosmin	No	No	No	No	No	No	No	No
Friedelin	No	Yes	No	No	No	No	No	No
Kaempferitrin	No	No	No	No	No	No	No	No
Luteolin	No	No	Yes	No	No	No	No	No
Myricitrin	No	No	No	No	No	No	No	No
Pseudo taraxasterol	No	Yes	No	No	No	No	No	No
Psi-taraxasterol	No	Yes	No	No	No	No	No	No
Quercetin	No	No	Yes	No	No	No	No	No
Rutin	No	No	No	No	No	No	No	No
α- amyrin	No	Yes	No	No	No	No	No	No
β- amyrin	No	Yes	No	No	No	No	No	No
β- amyrin acetate	No	Yes	No	No	No	No	No	No
3,5,7,3′,5′-Pentahydroxyflavone	No	No	Yes	Yes	Yes	No	No	No

Source: Own authorship, 2023.

The table presents interactions between various substances and enzymes in the CYP450 family. Substances such as β- amyrin acetate , friedelin , pseudo taraxasterol , bryotoxin A, α- amyrin , bryophyllin A, β- amyrin and psi-taraxasterol are substrates of the CYP3A4 enzyme, indicating that they undergo metabolism via this pathway. Furthermore, substances such as 3,5,7,3′,5′-pentahydroxyflavone, quercetin and luteolin have demonstrated interactions with CYP1A2 enzyme inhibitors, and it is important to note that only 3,5,7,3′,5′-pentahydroxyflavone, in addition to interacting with CYP1A2, it demonstrates interactions with inhibitors of the CYP2C19 and CYP2C9 enzymes.

The organic cation transporter 2 (OCT2) is a renal absorption transporter that plays a crucial role in the renal elimination of ionized forms of drugs and endogenous compounds, acting in the transfer of substances from the blood to the renal tubular cells, this being the first step in the process of elimination [60] . None of the selected compounds are expected to act as a substrate for OCT2.

The Ames toxicity test is a method widely used to predict the genotoxicity of compounds, especially regarding their mutagenicity, through the use of bacteria. Compounds predicted to be positive in the Ames test have the potential to induce mutagenicity [61] . Of the molecules analyzed, 13 presented negative results in the Ames test, indicating the absence of mutagenic activity. These substances are: bryotoxin B, β- amyrin acetate , diosmin , bryophyllin C, friedelin , pseudo taraxasterol , bryotoxin A, β- amyrin , psi-taraxasterol , kaempferitrin and luteolin . On the other hand, the compounds rutin, 3,5,7,3′,5′-

Pentahydroxyflavone, myricitrin , and astragalin obtained positive results, signaling mutagenic activity and, therefore, the possibility of acting as carcinogens (Table 7).

Table 7: Toxicity properties of *B. pinnatum compounds* with the best molecular interaction energies.

Compounds	**Toxicity**							
	AMES toxicity	**DMT (human) (LOG mg/kg/day)**	**hERG I inhibitor**	**hERG II inhibitor**	**TAO (rats) (LD50) (mol/kg)**	**TAO (rats) (LOAEL) (log mg/kg.bw/day)**	**Hepatotoxicity**	**Skin sensitization**
Astragalin	Yes	0.986	No	Yes	3,032	3,012	No	No
Bryophyllin A	No	-1.075	No	No	3,751	1,344	Yes	No
Bryophyllin C	No	-1,228	No	No	3,873	1,902	Yes	No
Bryotoxin A	No	-1,184	No	No	3,526	2,256	No	No
Bryotoxin B	No	-1,363	No	No	3,616	2,285	Yes	No
Diosmin	No	0.723	No	Yes	2,788	4,987	No	No
Friedelin	No	-0.374	No	Yes	2,502	0.87	No	No
Kaempferitrin	No	0.695	No	Yes	2,759	4,137	No	No
Luteolin	No	0.975	No	No	2.45	1,833	No	No
Myricitrin	Yes	0.68	No	Yes	2,771	3.31	No	No
Pseudo taraxasterol	No	-0.555	No	Yes	2,308	0.832	No	No
Psi-taraxasterol	No	-0.555	No	Yes	2,308	0.832	No	No
Quercetin	Yes	0.954	No	No	2,308	3,134	No	No
Rutin	Yes	0.55	No	Yes	2,523	4,415	No	No
α- amyrin	No	-0.607	No	Yes	2,288	0.848	No	No
β- amyrin	No	-0.596	No	Yes	2.3	0.866	No	No
β- amyrin acetate	No	-0.538	No	Yes	2,258	2,073	No	No
3,5,7,3′,5′-Pentahydroxyflavone	Yes	0.755	No	No	2,432	2.91	No	No

Source: Own authorship, 2023.

Note: T.AMES: AMES toxicity; DMT: maximum tolerated dose in humans; TAO: Acute Oral Toxicity in Rat; TCO: Chronic oral toxicity in rats; S.Skin : skin sensitization.

Acute oral toxicity in rats refers to the estimated LD50 value (lethal dose for 50% of animals) of a specific compound, indicating the amount in mol/kg of the substance necessary to cause the death of half of the animals tested. All compounds exhibited high values in this context. Among them, β- amyrin acetate recorded the lowest LD50, with a value of 2,258 mol/kg.

On the other hand, chronic oral toxicity in rats involves identifying the LOAEL (lowest observable adverse effect level) for a given compound. This value points to the lowest dose of the substance capable of inducing a detectable adverse effect. In the set of compounds tested, diosmin presented the most notable value, reaching 4,987 mol/kg.

The Maximum Tolerated Dose (MRTD) provides an estimate of the toxic dose in humans. The model predicts the logarithm of the MRTD for the analyzed compound. If the resulting value is equal to or less than 0.477 log (mg/kg/day), it is classified as a low dose; if it is greater than 0.477 log (mg/kg/day), it is categorized as a high dose [24] . Among the compounds evaluated, bryotoxin A, diosmin , bryophyllin C, friedelin , pseudo taraxasterol , bryotoxin A, α- amyrin , bryophyllin A, β- amyrin , psi-taraxasterol demonstrated low values, therefore indicating low toxicity. On the other hand, the remaining compounds analyzed showed high values.

No compound has been shown to be likely to cause skin sensitization. This is an adverse effect for products applied to the dermis. The assessment that a compound, when in contact with the skin, may induce allergic dermatitis is an important safety concern.

Liver toxicity is a significant concern during the drug development process as it can result in serious effects such as drug-induced liver injury resulting in acute liver failure, possibly requiring liver transplantation or resulting in death [62] . The molecules bryotoxin B, bryophyllin C and bryotoxin A showed signs of potential to trigger some form of liver dysfunction, which could result in liver damage.

The potassium channel through the human ether-a-go-go gene (hERG) is associated with the risk of developing long QT syndrome, which can culminate in sudden death. As a result of this inhibition, hERG is considered a relevant anti-target that should be avoided during the drug development process [63] . Consequently, the analysis revealed that none of the compounds has the ability to inhibit hERG I, in contrast to hERG II, where eleven compounds were identified as inhibitors: β- amyrin acetate , diosmin , friedelin , pseudo taraxasterol , α- amyrin , rutin, β- amyrin , psi-taraxasterol , kanferythrin , myricitrin and astragalin .

4. CONCLUSION

The present study provided satisfactory results in the molecular docking process in the interaction analysis of *B. pinnatum (Lam .)* Oken , with the main targets of SARS-COV-2, resulting in a total of 21 constituents with great inhibitory potential for the viral action of the coronavirus. Among the compounds analyzed, bryotoxin B, β- amyrin acetate and diosmin stand out, which presented the best affinity parameter for the Spike protein, with diosmin also presenting the best affinity parameter for the ACE2 protein, resulting in favorable scores for carrying out future *in vitro* and clinical tests. In fact, it is worth highlighting that the results of molecular docking tests of chemical compounds from *B. pinnatum (Lam .)* Oken analyzed within the parameter showed superior results compared to drugs approved by Anvisa for all proteins tested. This indicates a promising potential of *B. pinnatum*compounds as potential SARS-CoV-2 inhibitors identified by molecular docking as promising therapeutic candidates

in the treatment against COVID-19, once their efficacy is proven, as they are abundant and easily available from natural sources.

In short, the comprehensive evaluation of ADMET parameters reveals valuable data on the therapeutic viability of compounds, their pharmacological activity and possible risks, playing a crucial role in the search for innovative and safe therapeutic approaches. However, it is imperative to highlight that a complete understanding of the mechanisms of action and interactions in a clinical context still requires further investigation, outlining a path forward to translate this knowledge into tangible benefits for patients.

REFERENCES

1. Florindo HF, Kleiner R, Vaskovich-Koubi D, Acúrcio RC, Carreira B, Yeini E, et al. Immune-mediated approaches against COVID-19. Nature Nanotechnology. 2020;15(8):630–45.
2. Zhou P, Yang X Lou, Wang XG, Hu B, Zhang L, Zhang W, et al. A pneumonia outbreak associated with a new coronavirus of probable bat origin. Nature. 2020; 579(7798):270–3.
3. Zhu N, Zhang D, Wang W, Li X, Yang B, Song J, et al. A Novel Coronavirus from Patients with Pneumonia in China, 2019. N Engl J Med. 2020;382(8):727–33.
4. Ciotti M, Angeletti S, Minieri M, Giovannetti M, Benvenuto D, Pascarella S, et al. COVID-19 Outbreak : An Overview. Chemotherapy . 2019;64(5–6):215–23.
5. Pushpakom S, Iorio F, Eyers PA, Escott KJ, Hopper S, Wells A, et al. Drug repurposing: progress, challenges and recommendations. Nat Rev Drug Discov. 2019;18(1):41–58.
6 Akindele AJ, Sowemimo A, Agunbiade FO, Sofidiya MO, Awodele O, Ade-Ademilua O, et al. Bioprospecting for anti-COVID-19 interventions from African medicinal plants: a review. Nat Prod Commun. 2022;17(5):1934578X221096968.
7. Brogi S. Computational Approaches for Drug Discovery. Molecules. 2019; 24(17).
8. Zaki AA, Ashour A, Elhady SS, Darwish KM, Al-Karmalawy AA. Calendulaglycoside A showing potential activity against SARS-CoV-2 main protease: Molecular docking, molecular dynamics, and SAR studies. J Tradit Complement Med. 2022;12(1):16–34.
9. Lin X, Li X, Lin X. A Review on Applications of Computational Methods in Drug Screening and Design. Molecules. 2020;25(6).
10. Afzal M, Kazmi I, Anwar F. Antineoplastic potential of Bryophyllumpinnatum lam. on chemically induced hepatocarcinogenesis in rats. Pharmacognosy Res. 2013;5(4):247.
11. Gil LS. Usosetno-medicinais de plantasnaNigéria. Benin: UNIBEN Press; 1992. 46 p.
12. Devbhuti D, Jk G, Devbhuti P. Studies on Antitumor Activity of BryophyllumcalycinumSalisb. against Ehrlich Ascites Carcinoma in Swiss Albino Mice. Journal of PharmaSciTech. 2012;2(1):31–3.
13. Akinpelu DA. Antimicrobial activity of Bryophyllumpinnatum leaves. Fitoterapia. 2000;71(2):193–4.
14. Ojewole JA. Antihypertensive properties of B. pinnatum (Lam) leaf extracts. AMJ Hipert. 2002;15(4):A34–9.
15. Al-Snafi AE. The Chemical Constituents and Pharmacological Effects of Bryophyllumcalycinum. A review. International Journal of Pharma Sciences and Research (IJPSR). 2013;4.
16. Obioma A, Chikanka AT, Dumo I. Antimicrobial Activity of Leave Extracts of Bryophyllumpinnatum and Aspiliaafricana on Pathogenic Wound Isolates Recovered from Patients Admitted in University of Port Harcourt Teaching Hospital. Ann Clin Lab Res. 2017; 5(3):185.

17. Rocha JA, Rego NCS, Carvalho BTS, Silva FI, Sousa JA, Ramos RM, et al. Computational quantum chemistry, molecular docking, and ADMET predictions of imidazole alkaloids of Pilocarpusmicrophyllus with schistosomicidal properties. PLoS One. 2018;13(6).
18. Meng XY, Zhang HX, Mezei M, Cui M. Molecular docking: a powerful approach for structure-based drug discovery. Curr Comput Aided Drug Des. 2011;7(2):146–57.
19. Berman HM, Westbrook J, Feng Z, Gilliland G, Bhat TN, Weissig H, et al. The Protein Data Bank. Nucleic Acids Res. 2000;28(1):235–42.
20. Barros RO, Junior FLCC, Pereira WS, Oliveira NMN, Ramos RM. Interaction of Drug Candidates with Various SARS-CoV-2 Receptors: An in Silico Study to Combat COVID-19. J Proteome Res. 2020;19(11):4567–75.
21. Pettersen EF, Goddard TD, Huang CC, Couch GS, Greenblatt DM, Meng EC, et al. UCSF Chimera - A visualization system for exploratory research and analysis. J. Comput. Chem. 2004;25(13):1605–12.
22. Trott O, Olson AJ. AutoDockVina: Improving the speed and accuracy of docking with a new scoring function, efficient optimization, and multithreading. J Comput Chem. 2009.
23. Wallace AC, Laskowski RA, Thornton JM. LIGPLOT: a program to generate schematic diagrams of protein-ligand interactions. Protein Engineering, Design and Selection. 1995;8(2):127–34.
24. Pires DEV, Blundell TL, Ascher DB. pkCSM: Predicting Small-Molecule Pharmacokinetic and Toxicity Properties Using Graph-Based Signatures. J Med Chem. 2015;58(9):4066–72.
25. Chun CY, Khor SXY, Chia AYY, Tang YQ. In silico study of potential SARS-CoV-2 antagonist from Clitoriaternatea. Int J Health Sci (Qassim). 2023;17(3):3.
26. Kamboj A, Saluja A, Saluja A, Saluja A. Bryophyllumpinnatum (Lam .) Kurz .: Phytochemical and Pharmacological Profile: A Review. Pharmacogn Rev. 2009;3(6).
27. Khooshbu P, Ansari I. A pharmacognostical and pharmacological review on Bryophyllumpinnatum (Panphuti). Asian J Pharm Clin Res. 2019;12(1):34–9.
28. Tatsimo SJN, Tamokou JDD, Havyarimana L, Csupor D, Forgo P, Hohmann J, et al. Antimicrobial and antioxidant activity of camppherolrhamnoside derivatives from Bryophyllumpinnatum . BMC Res Notes. 2012;5
29. Yadav P, Mishra AK, Singh H. A Recent Review on Chemistry and Biological Activities of BryophyllumPinatum (Lam.) Oken Family: Crassulaceae. Oriental Journal Of Chemistry. 2021;37(2):269–80.
30. Sobreira FC. Assessment of Kalanchoe Antiulcer Activity pinnata (Lam .) Pers (Crassulaceae). [Dissertation (Master's in Drugs and Medicines)]. [São Paulo]: University of São Paulo; 2013.
31. Fürer K, Simões-Wüst AP, Von Mandach U, Hamburger M, Potterat O. Bryophyllumpinnatum and Related Species Used in Anthroposophic Medicine: Constituents, Pharmacological Activities, and Clinical Efficacy. Planta Med. 2016;82(11–12):930–41.
32. Uchegbu RI. Chemical constituents analysis of the leaves of Bryophyllumpinnatum by GC-MS. AASCIT J Chem. 2017;3:19–22.
33. Hamming I, Timens W, Bulthuis MLC, Lely AT, Navis GJ, van Goor H. Tissue distribution of ACE2 protein, the functional receptor for SARS coronavirus. A first step in understanding SARS pathogenesis. J Pathol. 2004;203(2):631–7.
34. Yuniwati Y, Syaban MFR, Anoraga SG, Sabila FL. Molecular Docking Approach of BryophyllumPinnatum Compounds as Atherosclerosis Therapy By Targeting Adenosine Monophosphate-Activated Protein Kinase and Inducible Nitric Oxide Synthase. Acta Inform Med. 2022;30(2):91–5.

35 Rahman PA, Syaban MFR, Anoraga SG, Sabila FL. Molecular docking analysis from Bryophyllum pinnatum Compound as A COVID-19 cytokine storm therapy. Open Access Maced J Med Sci. 2022;10(B):779–84.
36. Krishnan K, Mathew LE, Vijayalakshmi NR, Helen A. Anti-inflammatory potential of β-amyrin, a triterpenoid isolated from Costusigneus. Inflammopharmacology. 2014;22(6):373–85.
37. Maurya R, Srivastava A, Shah P, Siddiqi MI, Rajendran SM, Puri A, et al. β-Amyrin acetate and β-amyrinpalmitate as antidyslipidemic agents from Wrightiatomentosa leaves. Phytomedicine. 2012;19(8–9):682–5.
38. Huwait E, Mobashir M. Potential and Therapeutic Roles of Diosmin in Human Diseases. Biomedicines. 2022;10(5).
39. Abdel-Reheim MA, Messiha BAS, Abo-Saif AA. Hepatoprotective effect of diosmin on iron-induced liver damage. International Journal of Pharmacology. 2017;13(6):529–40.
40. Pari L, Srinivasan S. Antihyperglycemic effect of diosmin on hepatic key enzymes of carbohydrate metabolism in streptozotocin-nicotinamide-induced diabetic rats. Biomed Pharmacother. 2010;64(7):477–81.
41. Kuntz S, Wenzel U, Daniel H. Comparative analysis of the effects of flavonoids on proliferation, cytotoxicity, and apoptosis in human colon cancer cell lines. Eur J Nutr. 1999;38(3):133–42.
42. Anand K, Ziebuhr J, Wadhwani P, Mesters JR, Hilgenfeld R. Coronavirus main proteinase (3CLpro) structure: basis for design of anti-SARS drugs. Science. 2003;300(5626):1763–7.
43. Zhang L, Lin D, Sun X, Curth U, Drosten C, Sauerhering L, et al. Crystal structure of SARS-CoV-2 main protease provides a basis for design of improved α-ketoamide inhibitors. Science. 2020;368(6489):409–12.
44. Hilgenfeld R, Hilgenfeld CR. From SARS to MERS: crystallographic studies on coronaviral proteases enable antiviral drug design. FEBS J. 2014;281(18):4085–96.
45. Maffucci I, Contini A. In Silico drug Repurposing for SARS-CoV-2 Main Proteinase and Spike Proteins . J Proteome Res 2020;19(11):4637–48.
46. Salinas NSC, Sampaio PRP, Parente ATM. The normative production of regulatory agencies: limits for possible control of Anvisa's regulatory actions in response to Covid-19. Legislative Information Magazine: RIL. 2021;58(230):55–83.
47. Patel P, Cerqueira DM, Santos GML, de Lima Soares R, Sousa VD, Liberti L, et al. The Baseline Analysis of Regulatory Review Timelines for ANVISA: 2013-2016. The R Innov Regulate Sci . 2020;54(6):1428–35.
48. ANVISA. National Health Surveillance Agency. Resolution RDC No. [9] , of February 20, 2015. Provides for the regulations for carrying out clinical trials with medicines in Brazil. Brasília, DF: DiárioOficialUnião; 2015.
49. ANVISA. Approved medicines — National Health Surveillance Agency - Anvisa [Internet]. 2021 [cited 2023 Sep 26]. Available from : https://www.gov.br/anvisa/pt-br/assuntos/paf/coronavirus/medicamentos
50. Daina A, Michielin O, Zoete V. SwissADME: a free web tool to evaluate pharmacokinetics, drug-likeness and medicinal chemistry friendliness of small molecules. Sci Rep. 2017;7.
51. Fatima S, Gupta P, Sharma S, Sharma A, Agarwal SM. ADMET profiling of geographically diverse phytochemical using chemoinformatic tools. Future Med Chem. 2020;12(1):69–87.
52. Jorgensen WL, Duffy EM. Prediction of drug solubility from structure. Adv Drug Deliv Rev. 2002;54(3):355–66.
53. Press B, Di Grandi D. Permeability for intestinal absorption: Caco-2 assay and related issues. Curr Drug Metab. 2008;9(9):893–900.

54. Belal A. Drug likeness, targets, molecular docking and ADMET studies for some indolizine derivatives. Pharmazie. 2018;73(11):635–42.
55. dos Saints Nunes L, Lilian Carvalho Gomes J, Patricia dos Saints Martins H, FaniDolabela M. In silico study of the activities of isolated compounds of Bauhinia variegata Linn . Research , Society and Development _ 2020;9(12).
56. Zhong HA. ADMET properties: Overview and current topics. Drug Design: Principles and Applications. 2017;113–33.
57. Flores-Holguín N, Frau J, Glossman-Mitnik D. Computational Pharmacokinetics Report, ADMET Study and Conceptual DFT-Based Estimation of the Chemical Reactivity Properties of Marine Cyclopeptides. ChemistryOpen. 2021;10(11):1142.
58. Nebert DW, Russell DW. Clinical importance of the cytochromes P450. Lancet. 2002;360(9340):1155–62.
59. Wolf CR, Smith G, Smith RL. Science, medicine, and the future: Pharmacogenetics. BMJ : British Medical Journal. 2000;320(7240):987.
60. Chen Y, Zhang S, Sorani M, Giacomini KM. Transport of paraquat by human organic cation transporters and multidrug and toxic compound extrusion family. J PharmacolExpTher. 2007;322(2):695–700.
61. Hansen K, Mika S, Schroeter T, Sutter A, Laak A Ter, Thomas SH, et al. Benchmark data set for in silico prediction of Ames mutagenicity. J Chem Inf Model. 2009;49(9):2077–81.
62. Chen M, Suzuki A, Borlak J, Andrade RJ, Lucena MI. Drug-induced liver injury: Interactions between drug properties and host factors. J Hepatol. 2015;63(2):503–14.
63. Sanguinetti MC, Tristani-Firouzi M. hERG potassium channels and cardiac arrhythmia. Nature. 2006;440(7083):463–9.